Results in Materials 20 (2023) 100488

Contents lists available at ScienceDirect

Results in Materials

journal homepage: www.sciencedirect.com/journal/results-in-materials

Macroscopic material degradation model of Norway spruce clear wood for XFEM

Tamás Király [a,*], Zsolt Karácsonyi [a], Rudolf Polgár [b]

[a] Institute for Applied Mechanics and Structures, University of Sopron, H-9400, Sopron, Bajcsy-Zsilinszky u. 4., Hungary
[b] ELTE Technical Management and Community Development Nonprofit Ltd., H-1056, Budapest, Szerb u. 21-23, Hungary

ARTICLE INFO

Keywords:
XFEM
LEFM
Norway spruce
Earlywood and latewood
Damage initiation
ABAQUS
Edge detection

ABSTRACT

The study aims at investigating the failure behavior of Norway spruce clear wood specimens using XFEM by modeling earlywood and latewood growth rings. The growth ring pattern in the specimens are determined using a photo-analytical processing program. For the simulations, 6 damage initiation mechanisms were considered and the subroutines were implemented in the finite element solver ABAQUS. A normal vector to the crack surface is calculated for each damage mode, taking into account the orientation of the maximum and minimum principal stresses. The XFEM model and the material properties are calibrated based on experiments, where the edge-notched specimens were subjected to 3-point bending, tensile and compression tests. The goal is to determine the ultimate load, locate structural weakpoints and obtaining a realistic crack propagation path by means of XFEM.

1. Introduction

Wood is a highly anisotropic and inhomogeneous material with a complex fiber structure. At the present there are several material models for the description of the mechanical properties and the failure modes of wood (see Fig. 1).

The work of P. C [1] provides a good overview about the fracture of solid wood and focuses on the structure and properties of wood at different length scales. The present work focuses on the failure behavior of the wood using an user defined damage initiation and damage evolution criterion at a macroscopic level. Like stated by Ref. [2]; wood shows ductile behavior in compression and brittle behavior in tension and shear, where both failure modes can occur simultaneously. They propose an inhomogeneous and orthotropic material model that can identify 8 stress-based failure modes and combine ductile and brittle failures. The results were satisfying in terms of stiffness and load carrying capacity. A better prediction could be achieved by capturing the relevant details like grain patterns combined with a more complex material model.

Some compared different methods for the prediction of strength behavior of wood by investigating the wood in different scales [3]. They also applied XFEM (eXtended Finite Element Method) for early- and latewood unit cells to understand the complex failure mechanisms.

For the macroscopic FE-models, the rule of mixtures and the two phases of wood, earlywood and latewood were considered, based on a previous research [4]. The predictive capabilities of the material model strongly depend on their calibration, that means using input parameters obtained with a set of experimental data. The required mechanical material parameters were determined based on the experiments conducted and other researches, such as [2,5,6]; [1,3].

In some cases, which are determined by the direction of loading, wood behaves mainly like a brittle material, so that linear elastic fracture mechanic principles based on the fracture toughness parameter K_{IC} are able to characterize the fracture process adequately [7]. The critical stress intensity factor K_{IC} and the critical energy release rate G_C are used for characterizing linear elastic fracture mechanic quantities, because stress- and strain-based methods are not suitable in situations where large stress or strain concentrations occur. According to Ref. [7]; it is nowadays also commonly accepted that wood may be treated as a quasi-brittle material.

The novelty of this research is that XFEM with linear elastic fracture mechanics is used to describe the crack initiation and propagation, distinguishing between earlywood and latewood in bulk, each with a characteristic orthotropic material behavior. 6 damage initiation criteria are used to describe the failure mechanisms of the Norway spruce (*Picea abies*) clear wood specimens. A normal vector to the crack surface is

* Corresponding author.
E-mail addresses: kiraly.tamas@phd.uni-sopron.hu (T. Király), karacsonyi.zsolt@uni-sopron.hu (Z. Karácsonyi), polgar.rudolf@sek.elte.hu (R. Polgár).

https://doi.org/10.1016/j.rinma.2023.100488
Received 2 September 2023; Received in revised form 24 October 2023; Accepted 9 November 2023
Available online 23 November 2023

calculated for each damage mode, taking into account the orientation of the maximum and minimum principal stresses. The damage initiation criteria is coded in FORTRAN for the finite element solver ABAQUS [8].

2. Theory of XFEM

The developement of the XFEM came a long way since its introduction by Refs. [9,10] based on the partition of unity proposed by Ref. [11]. The XFEM allows the presence and propagation of cracks without the need for the mesh to match the crack path. Thus, XFEM is an excellent tool for the LEFM (linear elastic fracture mechanics) to simulate failure. It is more suitable for brittle fracture and can also be used when there is no initial crack.

The advantage of LEFM is that due to the linearity of the constitutive equations and because of the assumption of small strains, closed form solutions for stress and strain fields at a crack tip can be obtained [12]. These assumptions do not apply for incremental plasticity, because the constitutive equations are non-linear, moreover, the current stress-strain state depends on the loading history.

LEFM is suitable for problems with small-scale yielding, which means that the zone of plasticity is small compared to the crack size.

XFEM is able to achieve optimal convergence rates on structured meshes, where arbitrary discontinuities and singularities exist within the elements. There are two different types of discontinuities which should be considered: in case of a weak discontinuity the gradient has a jump and in case of a strong discontinuity the field quantity has a jump.

Through the use of level-set method in ABAQUS [8], the location of discontinuities with respect to the existing mesh is determined.

A level-set function is a scalar function within the domain whose zero-level is interpreted as the discontinuity [13]. The combination of XFEM with the level-set method allows the representation of an arbitrary 3D crack, where the crack is completely described by nodal data.

XFEM allows the presence of discontinuities in an element by enriching the degrees of freedom with special displacement functions, shown in eq. (1). The displacement function consists of a standard FE (finite element) approximation part $\mathbf{u}^{FE}$ and an enrichment $\mathbf{u}^{enr}$ [10]:

$$\mathbf{u} = \mathbf{u}^{FE} + \mathbf{u}^{enr} = \sum_{I=1}^{N} N_I(x) \cdot \left[\mathbf{u}_I + H(x) \cdot \mathbf{a}_I + \sum_{\alpha=1}^{4} F_\alpha(x) \cdot \mathbf{b}_I^\alpha \right] \tag{1}$$

where $\mathbf{u}$ displacement vector, $N_I(x)$ shape functions, $\mathbf{u}_I$ nodal displacement vectors, $H(x)$ jump function, $\mathbf{a}_I$ nodal enriched degree of freedom vector, $F_\alpha(x)$ asymptotic crack-tip function, $\mathbf{b}_I^\alpha$ nodal enriched degree of freedom vector. The terms in eq. (1) have the following function [10]:

1. Term: $N_I(x) \cdot \mathbf{u}_I$, applies to all nodes in the model;
2. Term: $N_I(x) \cdot H(x) \cdot \mathbf{a}_I$, applies to nodes whose shape function support is cut by the crack interior;
3. Term: $N_I(x) \cdot \left[\sum_{\alpha=1}^{4} F_\alpha(x) \cdot \mathbf{b}_I^\alpha \right]$, applies to nodes whose shape function support is cut by the crack tip.

For this research the XFEM based cohesive segments method is used to simulate the crack initiation and propagation, where only the displacement jump across a cracked element is considered. For propagation cracks the third term in eq. (1) is neglected, therefore the near-tip singularity is not considered. The crack must propagate over an entire element at once to avoid consideration of the stress singularity.

In order to represent the discontinuity of the crack, phantom nodes are introduced [14]. The phantom nodes are overlaid on the original ones and they stay connected to each other while the element is intact. The element intersected by a crack divides into two parts. Both parts consist of a combination of real and phantom nodes depending on the orientation of the crack.

However, according to the ABAQUS User Manual [8], there are limitations to the enriched function. Important limitations are that an enriched element cannot be intersected by more than one crack and that the crack is not allowed to turn more than 90° in one increment during an analysis. Also, some techniques are not supported, like adaptive remeshing and import analysis or elements like composite solid elements.

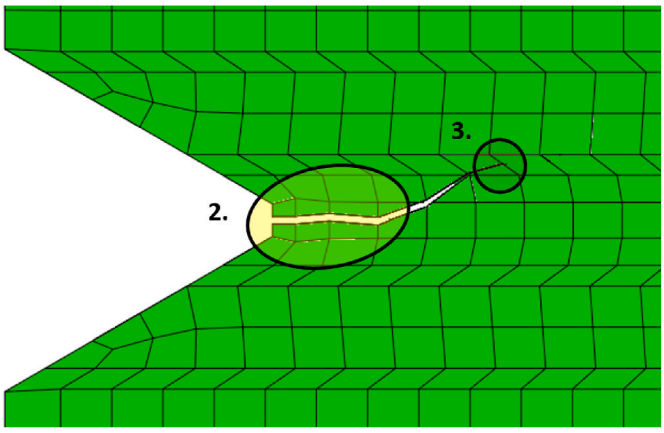

Fig. 1. Displacement vector of enriched elements, see eq. (1).

3. Material

3.1. Brief overview of the mechanical behavior of wood

The wood as a material has a cylindrical symmetry and can be described as an orthotropic material. Its three mutually perpendicular axes are [15]: longitudinal direction along the axis, radial and tangential directions in the transverse plane.

On a macroscopic scale the growth ring are differentiated. Their influence on the quality of wood is quite strong, and they must be treated separately. Therefore, it is of great interest to determine the ratio of earlywood and latewood in the bulk. The macroscopic properties of wood, such as density, hardness and other properties, are derived from the cells that make up the wood [16].

The wood of lower density is produced early in the season, therefore it is called earlywood. The earlywood contains larger lumina and thinner cell walls than the latewood. The cells of the latewood are densely layered and their walls are stronger and thicker.

This is due to the colder temperatures and drier conditions. The transition from earlywood to latewood is abrupt, usually without a distinct transition-zone [16]. In this research prime grade small Norway spruce specimens are investigated. None of the specimens have a major visible defect, drying splits or even knots, which is a natural feature of the species. This is mainly a FE-modeling issue that will be addressed in future development of the damage initiation and evolution of Norway spruce timber beams.

3.2. Damage initiation

The damage initiation is the point at which material properties are

Table 1
Description of the material constants for the failure criteria.

variable	description
$f_{t,R}$	tensile failure stress in radial direction
$f_{c,R}$	compressive failure stress in radial direction
$f_{t,T}$	tensile failure stress in tangential direction
$f_{c,T}$	compressive failure stress in tangential direction
$f_{t,L}$	tensile failure stress in longitudinal direction
$f_{c,L}$	compressive failure stress in longitudinal direction
$f_{s,L}$	failure shear stress in longitudinal direction
$f_{s,Q}$	failure shear stress in transverse direction

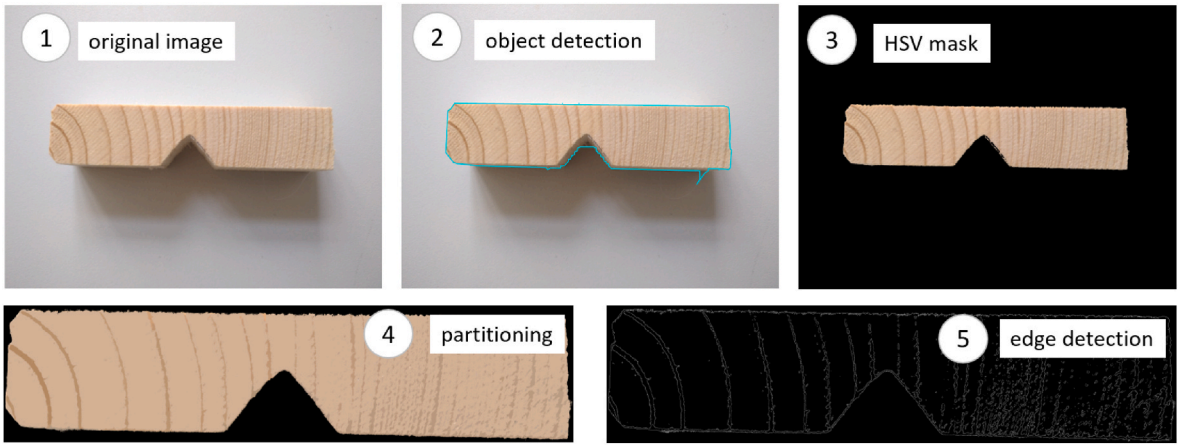

Fig. 2. Process of growth ring detection: 1) original image with background, 2) mask background with object detection algorithm, 3) use an HSV mask to cut out all unnecessary details, 4) partitioning algorithm to separate earlywood and latewood, 5) edge detection to get the contours.

first affected. In fracture mechanics of solids, three pure modes of crack propagation are considered [17]:

- mode I - tensile mode, where crack surfaces move directly apart,
- mode II - sliding (in-plane shear mode), where crack surfaces slide across one another in the direction perpendicular to the crack,
- mode III - tearing (antiplane shear mode), where the crack surfaces move parallel to the crack.

In addition, there is the so called mixed-mode fracture, which involves a combination of two to three of the modes.

The failure prediction of wood is a complex issue. Many researchers published different approaches as a failure criterion for wood, like [2, 18–20] or [3]; but there is no general agreement for a best fit. Guindos [21] compared several failure criteria, i.e. Tsai-Hill, Tsai-Azzi, Norris, extended Yamada-Sun, Hoffmann, Hashin and Tsai-Wu, while varying the element size of the FE-model. Guindos considered a transversely isotropic material property and established Tsai-Hill as the best criterion for failure prediction. T. Akter & K. Bader [22] compared Hill's and Hoffman's failure criteria using experimental data.

The Tsai-Hill [23] criterion uses the average strength and it does not take into account the differences between tensile and compressive strength. A more advanced version of the Tsai-Hill criterion is the Hoffman criterion [24]. It distinguishes tension and compression, but according to the study of [21]; it does not always lead to better results. The Hashin criterion [25] allows the identification of parallel-perpendicular and tensile-compressive failure. This criterion is used for predicting various failure modes, such as fiber breakage in tension, fiber buckling in compression, matrix cracking and debonding. Hashin and Rotem proposed a criterion for plane stress state [25] and few years later the criterion was also extended for 3-D stress state [26]. The criterion of Hashin does not always fit the experimental results in the case of matrix compression well [27]. The proposed quadratic failure criteria means, that the failure plane of the matrix mode is the maximum transverse shear plane. In their own research report, they note that this fact seems unacceptable in general.

The mode I failure is considered to major cause for engineering failure (P. C [1]. The wood failure has often a significant mode II component and according to P. C [1] the majority of the researchers found it difficult to obtain values or relations for pure mode II failure. The reason for this is the low fracture toughness in mode I parallel to the grain [28] found that fracture energy values were significantly higher for mode III than for Mode I. Therefore, only mode I fracture toughness is considered in this research.

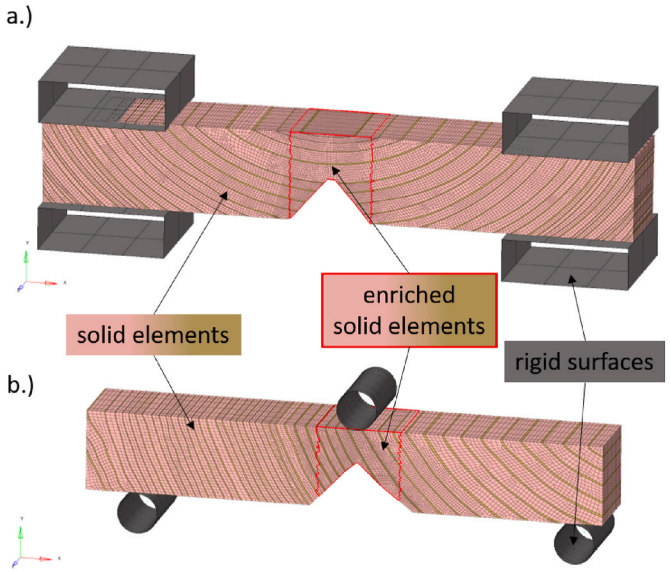

Fig. 3. Used element types of the FE models: a.) tensile test, b.) 3-point bending test.

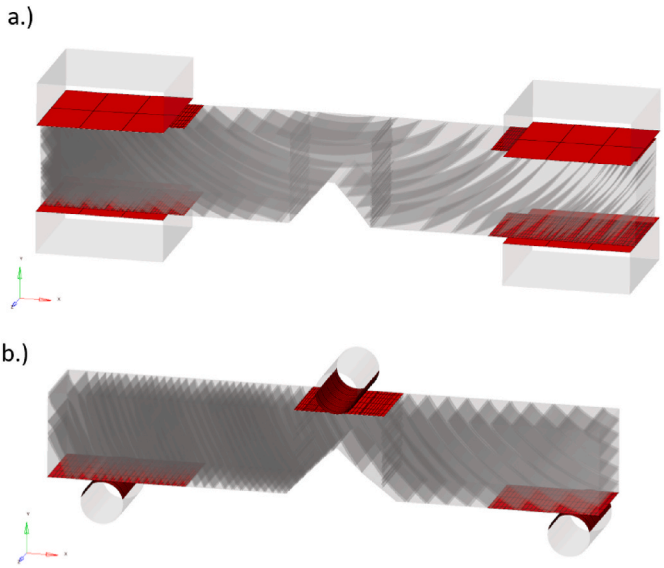

Fig. 4. Contact surfaces of the FE models: a.) tensile test, b.) 3-point bending test.

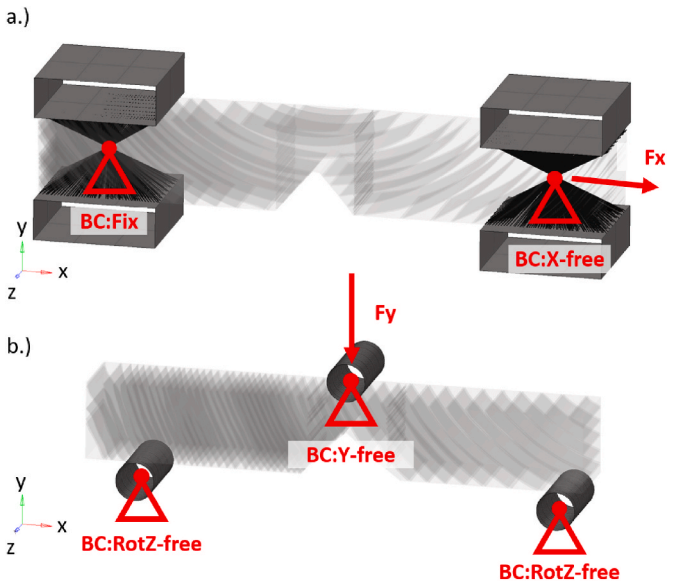

Fig. 5. Boundary conditions of the FE models: a.) tensile test, b.) 3-point bending test.

Table 2
Material properties of earlywood (EW) and latewood (LW) for Norway spruce used for the XFEM simulation.

material const.	symbol	unit	EW	LW	exponent
density	$\rho_{EW/LW}$	kg/m^3	258	984	–
long. modulus	$E_{L,\ EW/LW}$	MPa	4979,97	18993,37	1
rad. modulus	$E_{R,\ EW/LW}$	MPa	576,35	5108,91	1,63
tang. modulus	$E_{T,\ EW/LW}$	MPa	24,30	1348,13	3
Poissons's ratio LR	$\nu_{LR,\ EW/LW}$	–	0,041	0041	–
Poissons's ratio LT	$\nu_{LT,\ EW/LW}$	–	0,033	0033	–
Poissons's ratio RT	$\nu_{RT,\ EW/LW}$	–	0,350	0350	–
shear modulus LR	$G_{LR,\ EW/LW}$	MPa	387,43	1477,64	1
shear modulus LT	$G_{LT,\ EW/LW}$	MPa	394,11	1503,12	1
shear modulus RT	$G_{RT,\ EW/LW}$	MPa	44,65	2477,12	3

Table 3
Fracture toughness of Norway spruce considering the densitiy of early- and latewood.

variable	**values** $[MPa\cdot\sqrt{m}]$	
	EW	**LW**
$K_{IC,LR}$	1504	11,181
$K_{IC,LT}$		
$K_{IC,RL}$	0,136	1012
$K_{IC,TL}$		
$K_{IC,RT}$		
$K_{IC,TR}$		

Table 4
Energy release rates of Norway spruce for early- and latewood.

variable	**values** $[N/mm]$	
	EW	**LW**
$G_{f,L}$	0.452	6.582
$G_{f,R}$	0.032	0.200
$G_{f,T}$	0.759	0.759

The studies of other researchers show, that none of the failure criteria could predict a full failure envelope. The best suited criteria in one stress-state can lead to the worst prediction in another stress-state. One of the first criteria for wood was defined by Ref. [29]. Based on the fact, that the classical theory of plasticity is generally based on single-surface

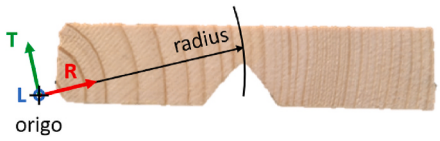

Fig. 6. Position of the cylindrical coordinate system and radius at the tip of the edge-notch.

failure criteria that are not able to identify single failure modes, he postulated 3 equations.

Based on the research results of T. Akter & K. Bader [2,22]; in this research 6 failure criteria are considered for clear wood (eqs. (2)–(7)), taking into account to following damage initiation mechanisms: tension and compression in the 3 main directions. In contrast to the aforementioned studies, these failure criteria are considered separately for the earlywood and latewood layers [2] also suggested pure shear failure modes, but these criteria seam to be obsolete, since the same shear components are also considered in the tensile failure mode in the direction perpendicular to the grain.

For each damage mode a normal vector to the crack surface $\bar{n}$ is assigned. Each wood species has its own fracture characteristic. In case of Norway spruce, the direction of the failure vectors was determined from the experiments conducted in Ref. [30]. After a series of parametric studies, it was found that there is a correlation between the direction of crack growth and the orientation of principal stresses in the finite element reached by the crack tip. The failure criteria are as follows:

- Damage initiation mode 1: Tensile failure mode in parallel-to-grain direction if $\sigma_{LL} \geq 0$. It is a maximum stress criterion:

$$\frac{\sigma_{LL}}{f_{t,L}} = 1 \tag{2}$$

The normal of failure vector is perpendicular to the maximum principal stress.

- Damage initiation mode 2 and 3: Tensile failure mode in perpendicular-to-grain direction if $\sigma_{RR} \geq 0$, respectively $\sigma_{TT} \geq 0$. The failure mode is caused by tensile stresses σ_{RR}, respectively σ_{TT} and shear stresses σ_{TL}, respectively σ_{RL} as well as rolling shear stress σ_{RT}. They are a quadratic criteria:

$$\left(\frac{\sigma_{RR}}{f_{t,R}}\right)^2 + \left(\frac{\sigma_{RT}}{f_{s,Q}}\right)^2 + \left(\frac{\sigma_{TL}}{f_{s,L}}\right)^2 = 1 \tag{3}$$

$$\left(\frac{\sigma_{TT}}{f_{t,T}}\right)^2 + \left(\frac{\sigma_{RT}}{f_{s,Q}}\right)^2 + \left(\frac{\sigma_{RL}}{f_{s,L}}\right)^2 = 1 \tag{4}$$

The normal of failure vector is perpendicular to the maximum principal stress.

- Damage initiation mode 4, 5 and 6: Compressive failure mode in parallel-to-grain direction if $\sigma_{LL} < 0$ and compressive failure mode in

Table 5
Failure stress values of Norway spruce.

variable	**values** $[MPa]$	
	EW	**LW**
$f_{t,R}$	1,15	3,50
$f_{c,R}$	−1,15	−3,50
$f_{t,T}$	4,30	12,00
$f_{c,T}$	−4,30	−12,00
$f_{t,L}$	60,00	126,00
$f_{c,L}$	−35,40	−58,00
$f_{s,L}$	3,40	6,50
$f_{s,Q}$	3,40	6,50

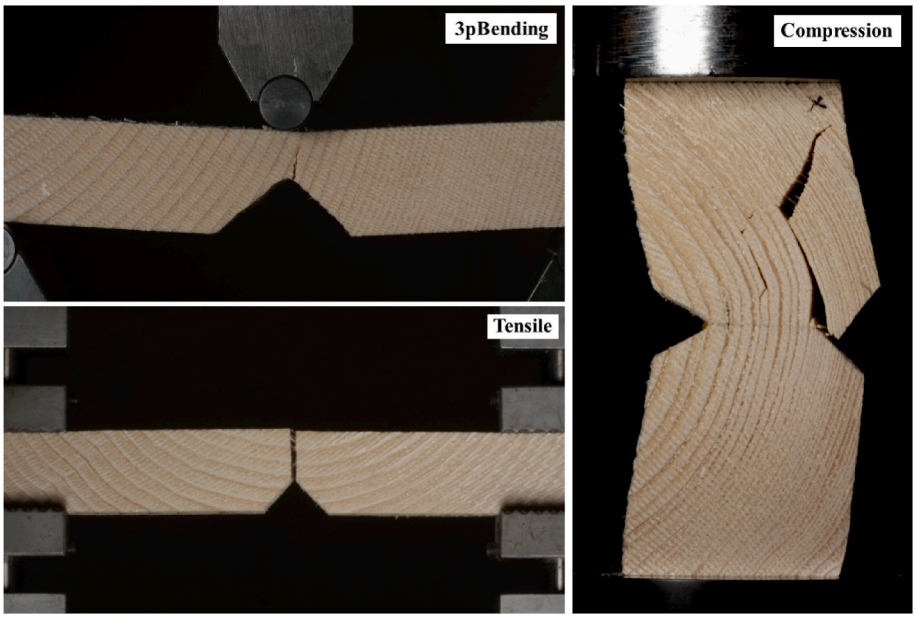

Fig. 7. Example of the tests: 3-point bending, tension and compression.

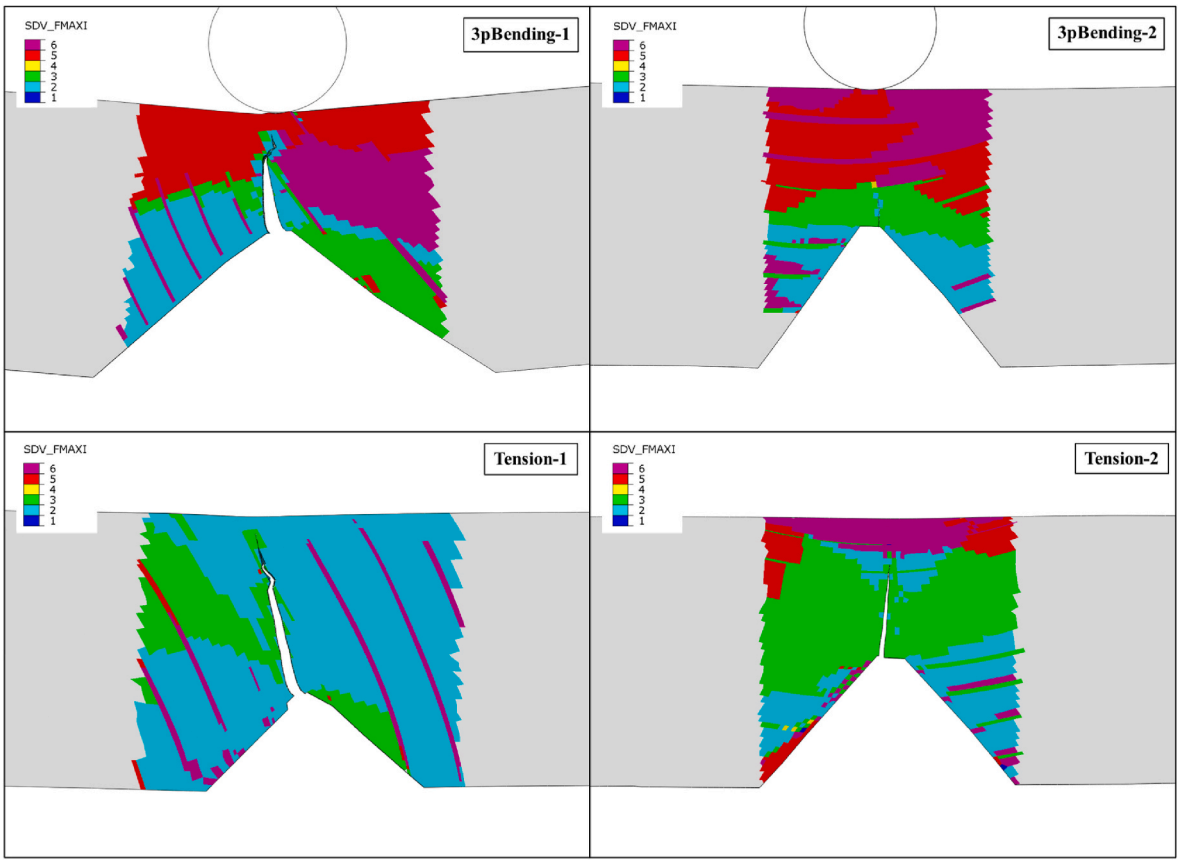

Fig. 8. Contour plot of the most critical damage criterion (SDV_FMAXI) per element.

Table 6
Naming convention and mode ID of the damage initiation criteria in the implemented FORTRAN subroutine.

variable	eq.	dam. mode	description
SDV_RFTL	eq. 2	1	tensile failure mode parallel-to-grain in longitudinal direction
SDV_RFTR	eq. 3	2	tensile failure mode perpendicular-to-grain in radial direction
SDV_RFTT	eq. 4	3	tensile failure mode perpendicular-to-grain in tangential direction
SDV_RFCL	eq. 5	4	compressive failure mode parallel-to-grain in longitudinal direction
SDV_RFCR	eq. 6	5	compressive failure mode perpendicular-to-grain in radial direction
SDV_RFCT	eq. 7	6	compressive failure mode perpendicular-to-grain in tangential direction

perpendicular-to-grain direction if $\sigma_{RR} < 0$, respectively $\sigma_{TT} < 0$. It is assumed that other stress components do not influence the tension strength [2]. They are a maximum stress criteria:

$$if\ \sigma_{LL} < 0 \qquad \frac{\sigma_{LL}}{f_{c,L}} = 1 \tag{5}$$

$$if\ \sigma_{RR} < 0 \qquad \frac{\sigma_{RR}}{f_{c,R}} = 1 \tag{6}$$

$$if\ \sigma_{TT} < 0 \qquad \frac{\sigma_{TT}}{f_{c,T}} = 1 \tag{7}$$

In case of σ_{LL} the normal vector is parallel and in case of σ_{RR} and σ_{TT} it is defined perpendicular to the minimal principal stress.

When at least one of the failure criteria is met, the damage initiation is triggered. The criterion that reaches the critical value earlier is responsible for the onset of failure. The list of material constants for the failure criteria is given in Table 1.

3.3. Damage evolution

The process of degradation begins when the stresses satisfy at least one of the defined crack initiation criteria, shown in eqs. (3)–(7). The criterion that has the highest value at the given timepoint is responsible for the failure.

The damage evolution defines the post damage-initiation material behavior and describes the rate of degradation of the material stiffness. The damage evolution law can be specified in terms of fracture energy (per unit area) or equivalent plastic displacement [18].

Stress fields in the vicinity of a crack tip can be characterized by a parameter, which is called the stress intensity factor and it is denoted by K_{IC} for the crack opening mode I. For an elastic and isotropic material [31] derived the relationship between the stress intensity factor K_{IC} and the strain energy release rate G_f. The equation for pure mode I is the following:

$$G_f = \frac{(K_{IC})^2}{E} \tag{8}$$

Later on [32] defined the relationship between K_{IC} and G_f for anisotropic materials. However, the simulations yielded more accurate results, when eq. (8) was used in conjunction with the defined damage initiation criteria:

$$G_{f,LL} = \frac{(K^a_{IC})^2}{E_{LL}} \tag{9}$$

$$G_{f,RR} = \frac{(K^n_{IC})^2}{E_{RR}} \tag{10}$$

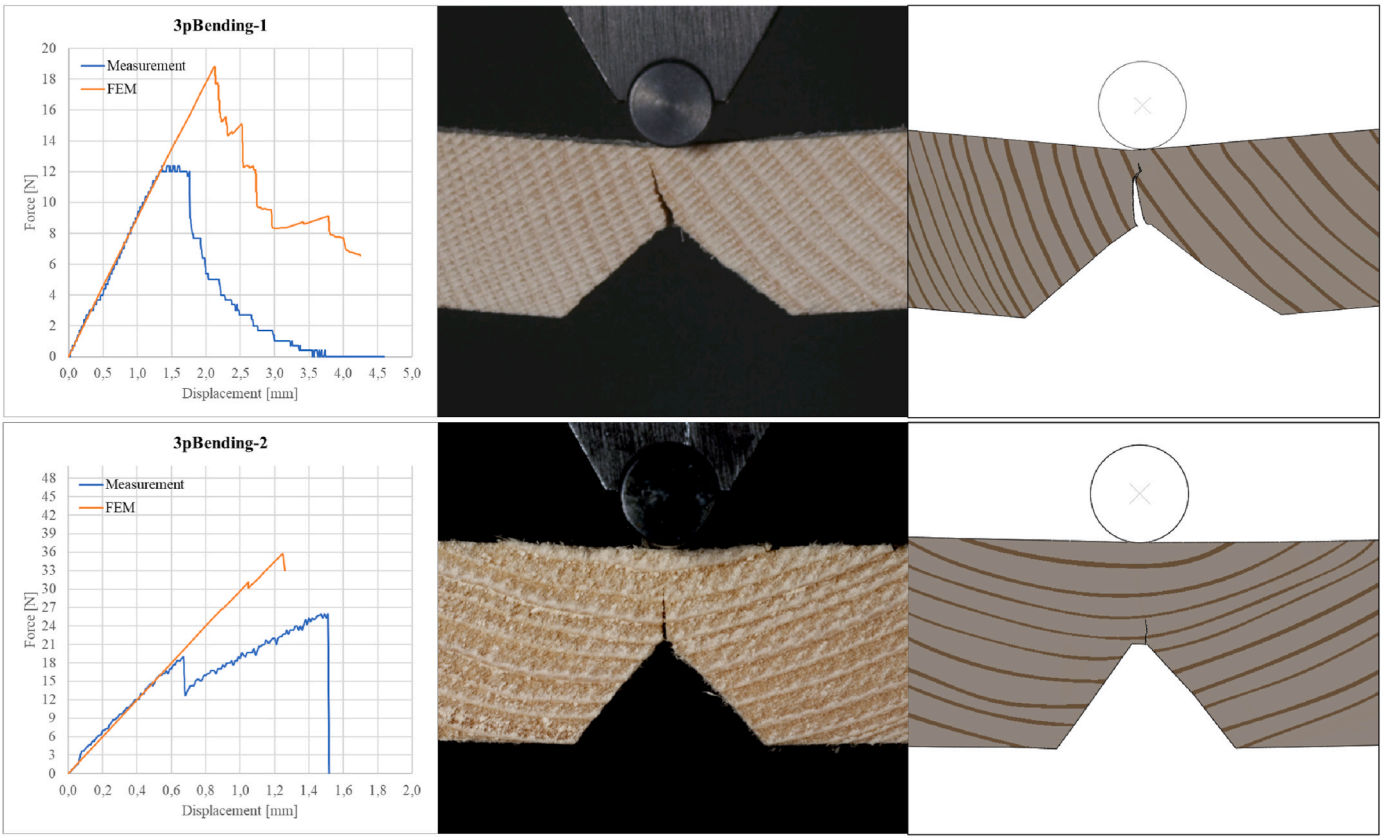

Fig. 9. Comparison of the measurement and XFEM results of the 3-point bending tests: force-displacement diagram (left), photo of measurement (middle), screenshot of XFEM (right).

Table 7
Summary table of measurement and XFEM results.

Basic information:			
Specimen	height at the notch [mm]	growth ring orientation at the notch [deg]	latewood ratio recognised by the tool [%]
3pBending-1	9,0	28,4	18,8
3pBending-2	9,3	90,0	24,7
Tension-1	13,0	33,5	32,3
Tension-2	10,1	90,0	24,1
Comparison of weight [g]:			
Specimen	measurement	FE model	difference in [%]
3pBending-1	18,8	18,2	−3,6 %
3pBending-2	24,7	19,5	−26,7 %
Tension-1	32,3	31,2	−3,5 %
Tension-2	24,1	22,9	−5,4 %
Comparison of ultimate load [N]:			
Specimen	measurement	XFEM	difference in [%]
3pBending-1	12,4	18,8	34,1 %
3pBending-2	26,0	35,7	27,2 %
Tension-1	382,4	393,5	2,8 %
Tension-2	332,4	388,7	14,5 %

$$G_{f,TT} = \frac{(K_{IC}^{n})^2}{E_{TT}} \tag{11}$$

Although fracture toughness has been measured for a wide range of species, there is no standard method for determining fracture toughness in any mode. The fracture toughness of wood increases with increasing density and relationships between density and K_{IC} can be postulated [33]:

$$K_{IC}^{n} = 20 \cdot \left(\frac{\rho}{\rho_s}\right)^{3/2} MPa \cdot \sqrt{m} \tag{12}$$

$$K_{IC}^{a} = 1.81 \cdot \left(\frac{\rho}{\rho_s}\right)^{3/2} MPa \cdot \sqrt{m} \tag{13}$$

where K_{IC}^{n} is the Mode I fracture toughness normal to the grain, K_{IC}^{a} is the Mode I fracture toughness along the grain, ρ is the wood density and ρ_s is the density of the cell wall material.

4. Finite element models

4.1. Modeling the growth ring pattern in the edge-notched specimens

In order to create the finite element models, a proprietary photo-analytical processing program was used to analyze the HSV color spectrum, detect objects and edges, thus detecting the growth ring pattern of the specimens on the images. There are some researchers presenting growth ring detection tools like [34,35] or [36]; but none of tools are currently freely available. Therefore, there was a need to develop such a tool with some advanced features for creating finite element models. The implemented algorithm uses the Canny edge detection, which is a multi-stage algorithm based on grayscale images developed by John F [37]. This technology is widely used today and has a variety of applications, such as the recognition of objects like traffic signs [38] or text recognition [39] [40].

The Canny edge detection algorithm consists of 6 steps: conversion the image to grayscale, noise reduction (Gaussian blur), gradient calculation for detecting the edge intensity, non-maximum suppression to thin out the edges, double threshold to filter out non-relevant edges and finally edge tracking by hysteresis to link edges. A subsequent spline fitting technique improves the contour of the result. The program tries to create edges with closed loops, which can be exported as a DXF (drawing interchange file format) file. For the detected edge loops, the surface can be calculated, and small surfaces can be filtered out if the user wishes.

The exported data can be imported in a FE preprocessor and the mesh can be created. Mesh-based preprocessors allow manipulation of the generated mesh, and in case of lack of details in the growth ring pattern or errors in the detected contour, the user can make the necessary adjustments.

Each of the annual rings identified in the specimen was assigned a circle with the approximate radius of the annual ring. The centers of the circles were then averaged and defined as the origin of the cylindrical coordinate system assigned to the specimen in the FE model.

To improve the performance of the tool detecting the growth rings, the specimens can be painted. The presented specimens were painted with a colorless nitro topcoat (Milesi LEC 040). The treatment does not affect the strength properties of the specimens, but it does highlight the growth rings. The treatment makes it easier for the photo-analytical program to distinguish between latewood and earlywood (see Fig. 2).

4.2. Description of the finite element models

The FE models were created in a mesh-based preprocessor (Altair Hypermesh) and calculated using the implicit static solver of ABAQUS [8]. The specimens were meshed with first order continuum elements C3D8I (8-node brick, hexahedral) as depicted in Fig. 3. In the area where the failure is expected, enriched finite elements are used. After the calculations, the results were carefully checked and it was ensured that the highest stresses, therefore the starting point of failure was certainly in the selected area. Nevertheless, the amount of enriched elements must be chosen reasonably in order to reduce the computation time. The stamps and clamps were meshed with R3D4 type rigid elements (4-node rigid shell) without thickness.

The interaction between specimen and stamps or clamps is established by small-sliding contact with friction. The defined contact surfaces are shown in Fig. 4. The defined contact interaction of cracked element surfaces is also based on the small-sliding formulation. In this formulation, the contact surfaces can undergo only a minor sliding relative to each other, but rotation of the bodies is permitted. Only static friction is considered in the simulations. Friction values for wood are given in scientific literature as 0,3–0,5 for dry and smooth wood against hard smooth surfaces, i.e. stamps and clamps [41]. The range of friction values for wood-on-wood is 0,25–0,55. Therefore, the general static friction coefficient was assumed to be 0,4 in the simulations.

Fig. 5 shows the boundary conditions for the tensile and 3-point bending tests. In the tensile tests, the clamps are fixed in all directions on one side, while on the other side displacement is only permitted in the

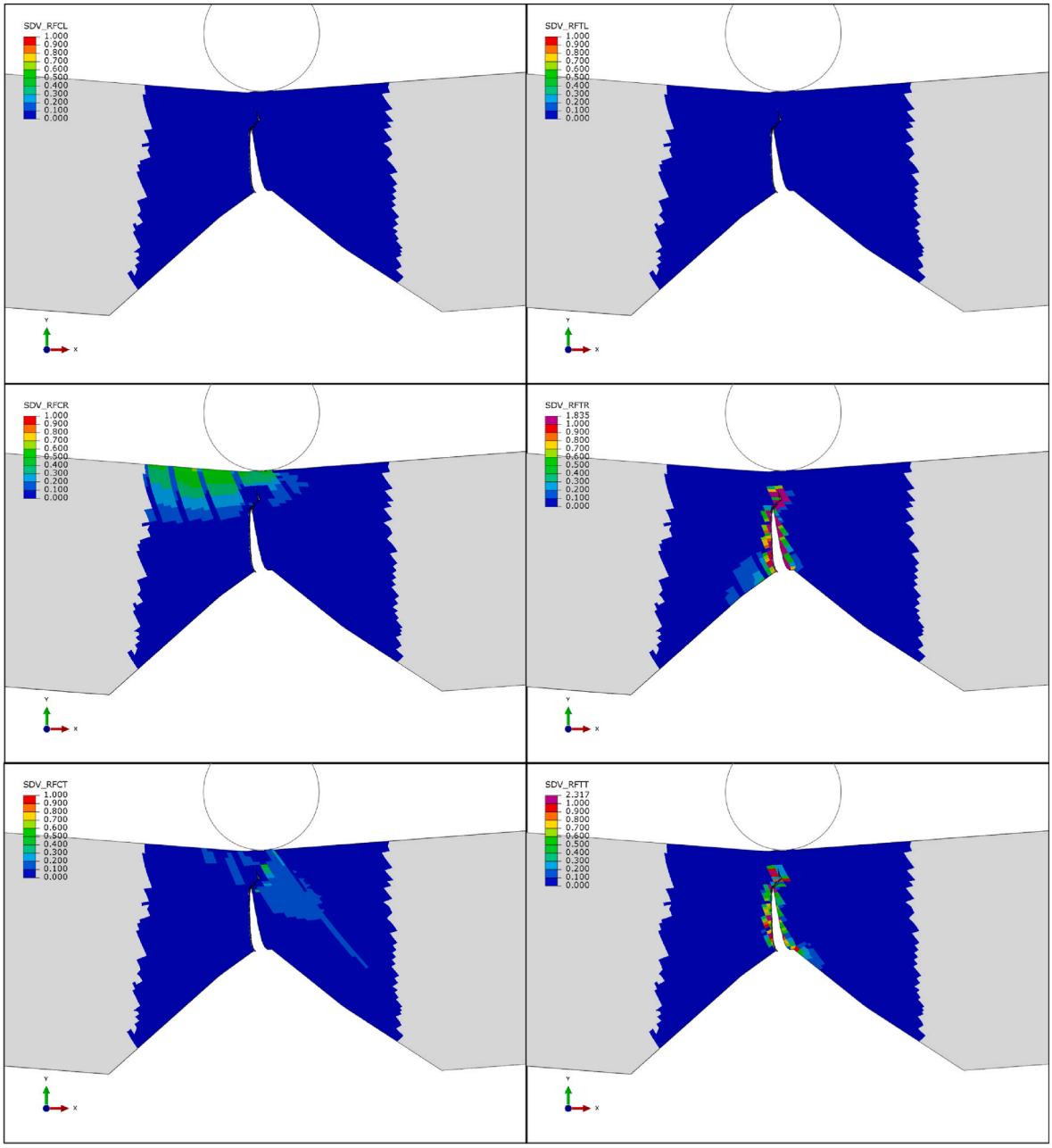

Fig. 10. Contour plot of the damage modes: as an example test specimen 3pBending-1.

x-direction. In the 3-point bending tests, the stamps on the bottom are fixed in all directions, but rotation about the z-axis is allowed, and the top stamp is also fixed, but displacement in the y-direction is permitted. The selected boundary conditions accurately represent reality.

4.3. *Material properties and degradation of spruce timber*

Currently there are no pre-selectable wood material models in ABAQUS [8] for FEM analyses considering material degradation, but there is a possibility to create user defined ones. ABAQUS uses several subroutines programmed in FORTRAN language to allow the user to define his own material degradation model. In our case, it was necessary to use the UDMGINI subroutine to implement the damage initiation criteria explained in chapter 3.2.

The first step is to define the orthotropic material model for the early- and latewood separately. This is done with the values of Table 2, which are the engineering constants associated with the material's principal directions. The method for determining the orthotropic material properties of earlywood and latewood, and the relationship between the density and strength of Norway spruce was presented in a previous publication [4]. The density of the earlywood and latewood of Norway spruce was determined by measuring finite small specimens. The density values listed in Table 2 were obtained for the batch of samples used for the investigation [30]. All of the specimens were sawn of Norway spruce (Picea abies) and dried to a moisture content of 12 %.

Next, the user-defined damage initiation criteria must be implemented. Each damage initiation mechanism is represented by a fracture criterion f_i (see eqs. (2)–(7)) and its associated normal direction to the crack plane. Crack initiation refers to the beginning of degradation of the cohesive response at an enriched element. Although there are 6 damage initiation mechanisms defined, the actual damage initiation for an enriched element is determined by the most severe damage initiation mechanism:

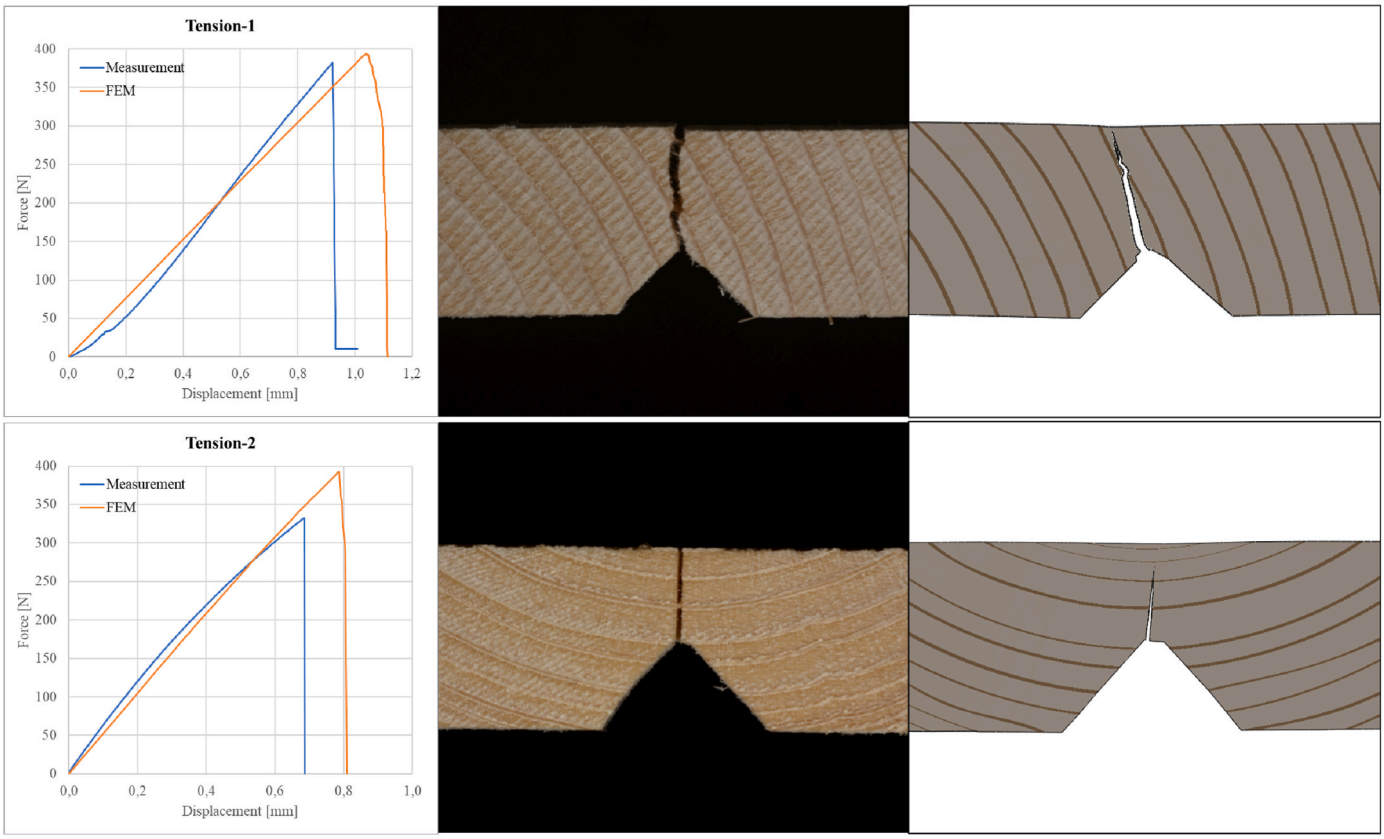

Fig. 11. Comparison of the measurement and XFEM results of the tensile tests: force-displacement diagram (left), photo of measurement (middle), screenshot of XFEM (right).

$$f = max(f_1, f_2, \ldots f_6) \tag{14}$$

Damage is initiated when f, as defined in equation (14), reaches the critical value of 1.0. An additional crack is introduced or the crack length of an existing crack is extended after an equilibrium increment when the fracture criterion, f, reaches the critical value within a given tolerance f_{tol} (by default 0.05) [8]:

$$1.0 \leq f \leq 1.0 + f_{tol} \quad (\text{where } f_{tol} \text{ is set } 0.01) \tag{15}$$

For the complete description of the damage process, the damage evolution must be defined in addition to the user-defined damage initiation criteria. It is possible to define a separate damage evolution law for each damage initiation criterion. Therefore, each combination of a damage initiation criterion with a corresponding damage evolution law is referred to as a failure mechanism. Damage is accumulated for only one failure mechanism per element, the mechanism whose damage initiation criterion was reached first in the increment. Deleting elements is possible in conjunction with XFEM, but it is not necessary because the XFEM elements split and the crack propagates.

The eqs. (12) and (13) and the density of the cell wall material can be used to calculate the fracture toughness of the earlywood and latewood, see Table 3. The mean mass density of the cell wall material of spruce timber is estimated at 1450 kg/m^3 [3].

In ABAQUS one can specify the fracture energy per unit area, G_f, to be dissipated during the damage process directly. If G_f is specified as 0, immediate failure would occur, which can lead to severe convergence issues. The values of G_f in Table 4 can be obtained by using eqs. (9)–(11), the material properties of earlywood and latewood defined in Table 2 and the K_{IC} values in Table 3.

4.4. Calibration of the material model

The predictive capabilities of the material model strongly depend on their calibration.

Subsequently, tests such as 3-point bending tests, tensile and compression tests were conducted until failure [30]. In each type of test 9 samples with different growth ring orientation were tested. The experiments were recorded with a high-resolution high-speed camera (Red Dragon 5 K sensor and Samyang 3.1/100 mm optics), where the failure mode and the crack path are clearly visible. The test results were evaluated afterwards and the results were reproduced with FE models. Linearelastic FEM calculations were performed, documenting the stress tensors of the finite elements in the area of the edge-notch, as well as the displacement and reaction force of the stamp or the clamp.

For the linear calculations, an optimization loop was performed in which the origin of the cylindrical coordinate system was varied so that the stiffness of the specimen in the FE model matched the calculated stiffness of the measurement with an error less than 5 %. The algorithm was allowed a maximum displacement of the origo of 10 % of the radius at the tip of the edge-notch of the specimen, like depicted on Fig. 6.

Another optimization loop, a parameter fitting, was used to determine the failure stresses of the Norway spruce. The stresses obtained were used to calculate the utilization of each damage initiation mode (eqs. (3)–(7)) for all finite elements in the area of the edge-notch. The values of [3] from Table 2 were used as initial values for the optimization. The goal of the optimization was to find the failure stresses at which the correct damage initiation criterion is activated at the correct location for all the specimens. The failure stresses used for the further XFEM calculations are listed in Table 5.

In the tests performed, the influence of radial, tangential and longitudinal failure stresses were the greatest. The values of the shear failure stresses have a relatively small influence on the utilization, but can make

a difference which damage initiation criterion is activated.

The specimens of the 3-point bending tests and the tensile tests fail dominantly with brittle fracture. The failure mode of these tests can be reproduced by the means of XFEM. However, in the compression test, a horizontal plateau is observed in the force-displacement curve, indicating a large elastoplastic deformation. For this reason, its failure behavior of Norway spruce cannot be adequately investigated by linear fracture mechanics. Examples of the 3 types of tests are shown in Fig. 7.

5. Results

After the 3 types of tests with 9 specimens each, additional test specimens were selected and tested. XFEM calculations were performed for these further specimens using the material values from Tables 2 and 5

The implemented FORTRAN subroutine differentiates between the acting most critical damage criteria in the enriched finite elements, see Fig. 8. From the results, it can be seen that the types of damage at the crack tip sometimes change from one element to another during deterioration. The criteria are recalculated for each integration point of each element at each iteration, until f does not reach 1.0. It may happen that from one increment to the next another criterion becomes more critical after a crack has occurred and the system does not give a linear response. The damage criteria are stored as solution dependent variables. Variable number 1 is the damage initiation mode 1 and so on, see the list of modes in Table 6.

The comparison of the results of the 3-point bending tests is shown in Fig. 9 and the tensile tests in Fig. 11 respectively. The origin of the cylindrical coordinate systems was determined by averaging the centers of the annual rings near the edge-notch. With this method, the stiffness was reproduced accurately with the FE models, see the force-displacement diagrams. However, the tougher challenge is to determine the ultimate load, which was less successful in the case of the 3-point bending tests than in the case of the tensile tests. A summary of the results can be found in Table 7.

In the case of the 3-point bending test, both the starting point of the crack and its initial path are well predicted by the XFEM calculation. For specimen *3pBending-1*, the ultimate load is overestimated with about 50 %. This is due to the fact that in the calculation the crack propagates through a latewood layer, while in reality the crack path only propagates in the earlywood layer. The Fig. 10 shows the acting damage criteria per element for this specimen. It can be clearly seen that the critical failure modes are tension in radial (SDV_RFTR) and tangential (SDV_RFTT) directions, which are alternately most critical as the crack progresses.

For specimen "3pBending-1″ the fracture energy plays a mayor role. It can be seen that after reaching the ultimate load, the horizontal plateau of the force-displacement curve is not accurately represented in the XFEM calculation, but the regression of the curve is correct with sufficient accuracy. In specimen "3pBending-2", failure occurs abruptly after the first two latewood layers crack. The XFEM calculation runs into convergence difficulties when calculating the contact under the stamp and it terminates earlier as defined.

For the specimen *3pBending-2*, the first earlywood layer fails at 19 N in the measurement and at 31 N in the XFEM calculation. Afterwards, the loss of stiffness in the XFEM model is lower, but the final failure occurs earlier than in the measurement. The stiffness values of the selected specimens in the 3-point bending tests are quite low, which makes this type of calculation particularly sensitive to modeling as well as to accurate material values.

The results of the tensile tests generally show a much better agreement than the 3-point bending test. The ultimate loads are overestimated by less than 20 % and the crack initiation points are predicted correctly in both cases. The crack path agrees with very good accuracy for the specimen "Tension-2". For specimen "Tension-1", the direction of crack growth is correct at the beginning, but in reality the crack reaches the latewood layer earlier. In this specimen, the failure modes tension in radial and tangential directions vary during the failure, resulting in a jagged crack path.

In the tensile test, the fracture energy plays a less important role than in the 3-point bending test, because of the brittle fracture. The simulations also converge better because there is no sliding in the contacts considered while deterioration.

6. Conclusion and summary

There is a growing need to combine the experimental data with finite element models to develop a material model that adequately represents the macroscopic failure behavior of wood.

The results of many researchers experimental campaigns show how difficult it is to determine the failure properties of wood, which are often system properties rather than material properties. In this research, XFEM with linear elastic fracture mechanics is used to describe the crack initiation and propagation. To describe the failure mechanisms of the Norway spruce clear wood specimens, 6 damage initiation criteria are used. A normal vector to the crack surface is calculated for each damage mode, taking into account the orientation of the maximum and minimum principal stresses. In examining the fracture of wood at the macro-level, no attempt is made to investigate the failure at lower levels of material structure, only the behavior under load. The predictive ability of the failure model is highly dependent on appropriate calibration. This work is related to Norway spruce. For other species, new measurements and calibrations are certainly required, but the species-specific failure model may also be necessary.

For the FE calculations, orthotropic material properties of earlywood and latewood, and the relationship between the density and strength of Norway spruce were used. To determine the failure properties for earlywood and latewood, 3-point bending, tension, and compression tests to failure were conducted. The experiments were recorded with a high-resolution highspeed camera, where the failure mode and the crack path is clearly visible. The force-displacement curves were also recorded and synchronized with the video footages. After obtaining the failure properties, further edge-notched specimens from the same batch were tested until failure. These specimens were also calculated using XFEM in ABAQUS, and the ultimate load and crack propagation in the specimens were compared with the measurement results. However, this required sufficiently accurate finite element models.

To create the finite element models, a photo-analytical processing program was used to detect the growth ring pattern of the specimens on the images.

The growth ring detection tools use the fact, that the brightness of the wood changes from the earlywood layer to the latewood layer. For this purpose, an object detection algorithm is used to detect the end grain cross section in the image and an edge detection algorithm is used to determine the annual rings.

In the 3-point bending tests, both the starting point of the crack and its initial path are well predicted by the XFEM calculation. In reality, however, the crack sometimes propagates between the earlywood and latewood layers in the transition zone. In such situations, the XFEM calculation overestimates the ultimate load. Considering the transition zone could be quite cumbersome, but a debonding mechanism between earlywood and latewood could be a possible simplified solution to obtain even more accurate results. The results of the tensile tests show an even better agreement than in case of the 3-point bending tests. The tensile specimens break with brittle fracture, so the fracture energy plays a less important role than in the 3-point bend tests. Also, no major sliding effects of the crack surfaces have to be considered, which generally leads to better convergence. The LEFM is only suitable for problems where the zone of plasticity is small compared to the crack size. However, there are studies on ductile and elasto-plastic fracture problems where strain-softening is considered to adequately capture larger plasticized areas. Overall, it can be stated that the use of a subroutine requires some expertise. The user is advised that the

implementation of a realistic constitutive model requires extensive development and testing.

The potential of the presented XFEM calculations can be used to build up a database for design and future model validation by investigating material failure behavior. For this purpose, the time-consuming model generation must be further automated. It is also time to explore new technologies such as artificial intelligence training with the collected databases so that more accurate results can be obtained with the FE models in the future.

Credit author statement

Tamás Király: Conceptualization, Methodology, Software, Validation, Formal analysis, Investigation, Data curation, Writing – Draft & Writing – review & editing, Visualization. Zsolt Karácsonyi: Supervision, Investigation (conducting experiment), Resources, Project administration, Funding acquisition. Rudolf Polgár: Supervision.

Declaration of competing interest

The authors declare that they have no known competing financial interests or personal relationships that could have appeared to influence the work reported in this paper.

Data availability

Data will be made available on request.

References

[1] P.C. Conrad, M.D. Smith, G, G. Fernlund, Fracture of solid wood: a review of structure and properties at different length scales, Wood Fiber Sci., J. Soc. Wood Sci. Technol. 35 (4) (2003) 570–584.
[2] C. Sandhaas, J. van de Kuilen, Material model for wood, Heron 58 (2013) 179–199.
[3] J. Füssl, M. Li, M. Lukacevic, C. Martin, Three Different Methods for Predicting the Strength Behaviour of Clear Wood - A Performance Comparison and Basis for a Combined Approach, 2016.
[4] T. Király, Z. Karácsonyi, R. Polgár, Modeling the earlywood and latewood growth rings of Norway spruce timber beams for finite element calculation, Wood Res. 68 (1) (2023) 28–43.
[5] J.A. Nairn, A numerical study of the transverse modulus of wood as a function of grain orientation and properties, Holzforschung 61 (4) (2007) 406–413.
[6] R.A. Luimes, A.S.J. Suiker, C.V. Verhoosel, A.J.M. Jorissen, H.L. Schellen, Fracture behaviour of historic and new oak wood, Wood Sci. Technol. 52 (2018) 1243–1269.
[7] S.E. Stanzl-Tschegg, P. Navi, Fracture behaviour of wood and its composites, Holzforschung 63 (2) (2009) 139–149.
[8] Dassault Systèmes, Abaqus 2020: Analysis User's Manual, 2019.
[9] T. Belytschko, T. Black, Elastic crack growth in finite elements with minimal remeshing, Int. J. Numer. Methods Eng. 45 (1999) 601–620.
[10] N. Moës, J. Dolbow, T. Belytschko, A finite element method for crack growth without remeshing, Int. J. Numer. Methods Eng. 46 (1999) 131–150.
[11] J. Melenk, I. Babuska, The partition of unity finite element method: basic theory and applications, Comput. Methods Appl. Mech. Eng. 39 (1996) 289–314.
[12] W. Brocks, Plasticity and Fracture, first ed., Springer, 2018.
[13] M. Stolarska, D.L. Chopp, N. Moës, T. Belytschko, Modelling crack growth by level sets in the extended finite element method, Int. J. Numer. Methods Eng. 51 (2001) 943–960.
[14] J.H. Song, P.M.A. Areias, T. Belytschko, A method for dynamic crack and shear band propagation with phantom nodes, Int. J. Numer. Methods Eng. 67 (2006) 868–893.
[15] J. Szalai, Anisotropic Elasticity and Strength of Wood and Wood-Based Materials, Part 1: Anisotropy of Echanical Properties [in Hungarian: A Faanyag És Faalapú Anyagok Anizotróp rugalmasság- És Szilárdságtana, 1. rész: A Mechanikai tulajdonságok Aniztrópiája, Hillebrand Nyomda, 1994.
[16] R. Ross, Wood Handbook: Wood as an Engineering Material, Centennial ed., USDA Forest Products Society, Madison, WI, 2010. Chapters 3 and 5.
[17] M. Janssen, J. Zuidema, R. Wanhill, Fracture Mechanics: Fundamentals and Applications, 2004.
[18] L. Le-Ngoc, H. McCallion, On the Fracture Toughness of Orthotropic Materials, vol. 58, Elsevier Science Ltd., Engineering Fracture Mechanics, 1997, pp. 355–362.
[19] L. Kyzioł, Analysis of Fracture Toughness of Structural Timber, vol. 17, POLISH MARITIME RESEARCH, 2010, pp. 53–58.
[20] F. De Megistris, L. Salmén, Finite Element modelling of wood cell deformation travsverse to the fibre axis, Mater. Sci., Nordic Pulp Paper Res. J. 23 (2015) 240–246.
[21] P. Guindos, Comparison of Different Failure Approaches in Knotty Wood, vol. 57, 2014, pp. 51–68.
[22] T. Akter, S, K. Bader, T, Experimental assessment of failure criteria for the interaction of normal stress perpendicular to the grain with rolling shear stress in Norway spruce clear wood, Wood Res. 78 (2020) 1105–1123.
[23] S.W. Tsai, in: R.T. Schwartz, H.S. Schwartz (Eds.), Strength Theories of Filamentary Structure. *Fundamental Aspects of Fiber Reinforced Plastic Composites*, Wiley Interscience, New York, 1968, pp. 3–11.
[24] O. Hoffman, The brittle strength of orthotropic materials, J. Compos. Mater. 1 (1967) 200–206.
[25] Z. Hashin, A. Rotem, A fatigue failure criterion for fiber reinforced materials, J. Compos. Mater. 7 (1973) 448–464.
[26] Z. Hashin, A. Rotem, Failure criterion for unidirectional fiber composites, ASME J. Appl. Mech. 47 (1980) 329–334.
[27] S. Pinho, C.G. Dávila, P.P. Camanho, L. Iannucci, Failure Models and Criteria for FRP under In-Plane or three-Dimensional Stress States Including Shear Non-linearity, Technical Report NASA Langley Research Center, Hampton, VA, 2005. NASA/TM-2005-213530.
[28] R.J.A. Ehart, S.E. Stanzl-Tschegg, E.K. Tschegg, Mode III fracture energy of wood composites in comparison to solid wood, Wood Sci. Technol. 33 (1999) 391–405.
[29] C.B. Norris, Strength of orthotropic materials subjected to combined stresses, in: Misc. Pub FPL-1816, U.S. Dept. of Agriculture, Forest Service, Forest Products Laboratory, Madison, Wis, 1962, p. 40.
[30] T. Király, Z. Karácsonyi, Fracture testing of edge-notched timber beams with different growth ring orientations, Wood Res. 68 (3) (2023) 558–571.
[31] G.R. Irwin, Analysis of stresses and strains near the end of a crack traversing a plate, J. Appl. Mech. 24 (1957) 361–364.
[32] G.C. Sih, P.C. Paris, G.R. Irwin, On cracks in rectilinearly anisotropic bodes, Int. J. Fract. Mech. 1 (1965) 189–203.
[33] M.F. Ashby, K.E. Easterling, R. Harryson, S.K. Maiti, The fracture toughness of woods, in: Proceedings of the Royal Society of London. Series A, Mathematical and Physical Sciences, vol. 398, 1985, pp. 261–280.
[34] M. Cerda, N. Hitschfeld, D. Mery, Robust tree-ring detection, in: Conference: Advances in Image and Video Technology, Second Pacific Rim Symposium, PSIVT 2007, 2007, pp. 575–585 (Santiago, Chile).
[35] T. Habite, O. Abdeljaber, A. Olsson, Automatic detection of annual rings and pith location along Norway spruce timber boards using conditional adversarial networks, Wood Sci. Technol. 55 (2021) 1–28.
[36] J. Van den Bulcke, E. Wernersson, M. Dierick, V. Denis, B. Masschaele, L. Brabant, M. Boone, L. Hoorebeke, K. Haneca, A. Brun, C. Luengo Hendriks, J. Van Acker, 3d tree-ring analysis using helical x-ray tomography, Dendrochronologia 32 (2013) 39–46.
[37] J.F. Canny, A computational approach to edge detection, IEEE Trans. Pattern Anal. Mach. Intell. 8 (1986) 679–698.
[38] A. Ruta, F. Porikli, S. Watanabe, Y. Li, In-vehicle camera traffic sign detection and recognition, Mach. Vis. Appl. 22 (2011) 359–375.
[39] M. Pietikäinen, O. Okun, Edge-based method for text detection from complex document images, in: Conference: Document Analysis and Recognition, 2001. Proceedings. Sixth International Conference, 2001, pp. 286–291.
[40] H. Cho, M. Sung, B. Jun, Canny text detector: fast and robust scene text localization algorithm, in: Conference: 2016 IEEE Conference on Computer Vision and Pattern Recognition (CVPR), 2016, pp. 3566–3573.
[41] U. Deta, N. Suprapto, H. Mubarok, A. Syaiful Adam, A. Kholiq, The Comparison of Static Friction Coefficient on Wood between the Combination of Wood-Metal Load System and Wood-Sand Load System, 2019, pp. 887–890.